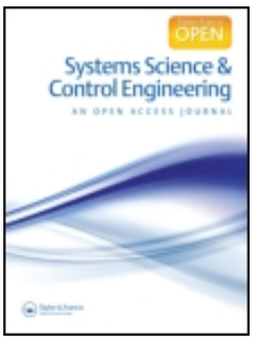

Systems Science & Control Engineering: An Open Access Journal

ISSN: (Print) 2164-2583 (Online) Journal homepage: https://www.tandfonline.com/loi/tssc20

A nonlinear oscillator with strange attractors featured Sinai-Ruelle-Bowen measure

Fengjuan Chen, Shujiao Jin & Liqun Zhou

To cite this article: Fengjuan Chen, Shujiao Jin & Liqun Zhou (2014) A nonlinear oscillator with strange attractors featured Sinai-Ruelle-Bowen measure, Systems Science & Control Engineering: An Open Access Journal, 2:1, 732-739, DOI: 10.1080/21642583.2013.879268

To link to this article: https://doi.org/10.1080/21642583.2013.879268

Systems Science & Control Engineering: An Open Access Journal, 2014
Vol. 2, 732–739, http://dx.doi.org/10.1080/21642583.2013.879268

Taylor & Francis
Taylor & Francis Group

A nonlinear oscillator with strange attractors featured Sinai-Ruelle-Bowen measure

Fengjuan Chen*, Shujiao Jin and Liqun Zhou

College of Mathematics, Physics and Information Engineering, Zhejiang Normal University, Jinhua, Zhejiang 321004, People's Republic of China

(*Received 13 September 2013; final version received 23 December 2013*)

This paper studies a class of Duffing oscillator with a forcing parameter ε. We obtain Hénon-like attractors, rank one attractors, and periodic sinks as ε changes. Hénon-like attractors and rank one attractors are chaotic in the sense of SRB measures, while periodic sinks represent stable dynamics with a basin of positive Lebesgue measure. As $\varepsilon \to 0$, three attractors construct a dynamical pattern repeating with certain period. Through numerical simulations, we observe three attractors perfectly as well as the dynamical pattern.

Keywords: homoclinic tangle; heteroclinic tangle; Hénon-like attractor; rank one attractor; SRB measure

1. Introduction

Duffing oscillator is known as a simple model displaying rich nonlinear dynamics, such as homoclinic tangles and horseshoes. In general, for an equation with homoclinic solution, periodic perturbation often leads to the intersection of stable and unstable manifolds. Therefore, Melnikov method is an efficient tool to detect horseshoes. However, it is possible for stable and unstable manifolds pulling apart. In this case, Melnikov method fails. Are there any important dynamics in this situation? What methods can be used to clear the important dynamics? How to deal with the intersection and pulling apart of stable and unstable manifolds together? Recently, Wang and Oksasoglu (2011) provided a complete theory on two-dimensional homoclinic tangles. With a new return map, they proved Hénon-like attractors and periodic sinks in homoclinic tangles beyond horseshoes. Further, for pulling apart, they obtained rank one attractors.

This paper studies a special class of Duffing oscillator, concentrating on its strange attractors as the forcing parameter changes. First, we present homoclinic solutions and heteroclinic solutions in unperturbed equation. Then, with double homoclinic tangle theory (Wang, 2009), we obtain Hénon-like attractors, rank one attractors, and periodic sinks, along with two dynamical patterns. With heteroclinic tangle theory (Chen, Oksasoglu, & Wang, 2013), we show Hénon-like attractors, periodic sinks, and transient tangles, also with a dynamical pattern. During this course, horseshoes are always participants, though we cannot observe it in numerical simulations.

2. Dynamics of perturbed homoclinic solutions

Although homoclinic tangles was discovered earlier by Poincaré (1899), the overall dynamics are far from understood. In Wang and Oksasoglu (2011), the authors presented a systematic study on homoclinic tangles for equation:

$$\begin{aligned} \frac{\mathrm{d}x}{\mathrm{d}t} &= f(x,y) + \varepsilon P(x,y,t), \\ \frac{\mathrm{d}y}{\mathrm{d}t} &= g(x,y) + \varepsilon Q(x,y,t), \end{aligned} \tag{1}$$

where $f(x,y)$, $g(x,y)$, $P(x,y,t)$, $Q(x,y,t)$ are $C^r (r \geq 3)$ functions, and $P(x,y,t+T) = P(x,y,t)$, $Q(x,y,t+T) = Q(x,y,t)$ for a constant $T > 0$.

Assume that the unperturbed equation, that is, $\varepsilon = 0$ in Equation (1), has a dissipative saddle point O connected with a homoclinic solution $\ell(t)$. If O is non-resonant, then a new return map R was derived in Wang and Oksasoglu (2011). Let Σ^- be a section, and (θ, x) be variables on Σ^-. Denote $(\theta_1, x_1) = \mathcal{R}(\theta, x)$. Then

$$\begin{aligned} \theta_1 &= \theta + a - \frac{\omega}{\beta} \ln F(\theta, x, \varepsilon) + \mathcal{O}_{\theta,x,h}(\varepsilon), \\ x_1 &= bF^{-\alpha/\beta}(\theta, x, \varepsilon), \end{aligned} \tag{2}$$

where a, b are constants, $\alpha < 0, \beta > 0$ are two eigenvalues of saddle O, and

$$F(\theta, x, \varepsilon) = \mathcal{W}(\theta) + kx + E(\theta, \varepsilon) + \mathcal{O}_{\theta,x,h}(\varepsilon). \tag{3}$$

*Corresponding author. Email: fjchen@zjnu.cn

In Equation (3), $\mathcal{W}(\theta)$ is a Melnikov function defined as

$$\mathcal{W}(\theta) = \int_{-\infty}^{+\infty} [P(\ell(t), t+\theta), Q(\ell(t), t+\theta)] \cdot \tau^{\perp}_{\ell(t)} e^{-\int_0^t \mathbb{E}_\ell(s)\,ds}\,dt, \tag{4}$$

k is a small constant, and $E(\theta,\varepsilon), \mathcal{O}_{\theta,x,h}(\varepsilon)$ are small error terms. In Equation (4), $\tau^{\perp}_{\ell(t)}$ is a vector perpendicular to the tangent vector of $\ell(t)$ at time t, and $\mathbb{E}_\ell(t)$ is the expansion rate of solutions in the neighborhood of $\ell(t)$.

From Equation (2), the domain of $\mathcal{R}$ depends on the image of $F(\theta,x,\varepsilon)$, which is related to the zeros of $\mathcal{W}(\theta)$. Denote

$$M = \max_{\theta\in S^1} \mathcal{W}(\theta), \quad m = \min_{\theta\in S^1} \mathcal{W}(\theta), \tag{5}$$

where $S^1 = \mathbb{R}/\{nT\}$ for $n \in \mathbb{Z}$.

THEOREM 2.1 (Wang, 2011; Wang & Oksasoglu, 2011)

(i) *If $\mathcal{W}(\theta)$ is a Morse function satisfying $m < 0 < M$, then Hénon-like attractors, periodic sinks, and horseshoes of infinitely symbols occur in the space of ε. Moreover, as $\varepsilon \to 0$, there is a dynamical pattern repeating with period $e^{\beta T}$, where β is the unstable eigenvalue of saddle O.*

(ii) *If $m > 0$, then rank one attractors occur for large ω, where ω is the frequency of perturbation.*

Remark 1 In Theorem 2.1(ii), $m > 0$ implies the pulling apart of stable and unstable manifolds. At this time, $\mathcal{R}$ defines on the full Σ^-. It is a rank one map admitting rank one attractors (Wang & Oksasoglu, 2008) characterized by SRB measures (Young, 2002; Benedicks & Young, 1993).

Denote two Melnikov functions by $\mathcal{W}^+(\theta)$ and $\mathcal{W}^-(\theta)$. Let

$$\begin{aligned} M^+ &= \max_{\theta\in S^1} \mathcal{W}^+(\theta), \quad m^+ = \min_{\theta\in S^1} \mathcal{W}^+(\theta), \\ M^- &= \max_{\theta\in S^1} \mathcal{W}^-(\theta), \quad m^- = \min_{\theta\in S^1} \mathcal{W}^-(\theta). \end{aligned} \tag{6}$$

THEOREM 2.2 (Wang, 2009; Wang & Oksasoglu, 2010) *Assume that $\mathcal{W}^+(\theta)$ and $\mathcal{W}^-(\theta)$ are two Morse functions.*

(i) *If $m^+, m^- < 0 < M^+, M^-$, then Equation (1) shows the mixture of two homoclinic tangles. It contains Hénon-like attractors, rank one attractors, and periodic sinks.*

(ii) *If $m^+ < 0 < M^+, m^- > 0$ (or $m^- < 0 < M^-$, $m^+ > 0$), then Equation (1) shows one homoclinic tangle and one rank one attractor. One-sided Hénon-like attractors, one-sided rank one attractors, and one-sided periodic sinks are created.*

(iii) *If $m^+ < 0 < M^+, M^- < 0$ (or $m^- < 0 < M^-$, $M^+ < 0$), then Equation (1) shows one tangle mixed with one rank one attractor. Hénon-like attractors, rank one attractors, and periodic sinks, including two-sided and one-sided, are permitted.*

(iv) *If $m^+ > 0, m^- > 0$, then Equation (1) shows two rank one attractors.*

(v) *If $m^+ > 0, M^- < 0$ (or $m^- > 0, M^+ < 0$ or $M^+ < 0, M^- < 0$), then Equation (1) shows only one rank one attractor.*

As $\varepsilon \to 0$, each case shows a repetitive dynamical pattern.

Remark 2 In Theorem 2.2, one-sided attractor means that the attractor is only on the left side or right side of saddle O. If it is on both sides, we call it two-sided attractor.

The setting of Theorems 2.1 and 2.2 are homoclinic solutions. Intuitively, heteroclinic cycle, formed by heteroclinic solutions, looks like a homoclinic loop. Therefore, perturbation to heteroclinic cycle also leads to complicated dynamics (Chen et al. 2013). Precisely, given two saddles O and O_*, connecting with two heteroclinic solutions $\ell(t)$ and $\ell_*(t)$ in unperturbed equation of (1). Let $\mathcal{W}(\theta)$, $\mathcal{W}_*(\theta)$ be two Melnikov functions with four extrema M, m, and M_*, m_*. We have

THEOREM 2.3 (Chen et al. 2013) *Suppose $\mathcal{W}(\theta)$ and $\mathcal{W}_*(\theta)$ are two Morse functions satisfying $m < 0 < M$, $m_* < 0 < M_*$, and O, O_* are both dissipative and non-resonant saddles. Then, Hénon-like attractors, periodic sinks, and horseshoes of infinitely many symbols occur for Equation (1) as $\varepsilon > 0$ changes.*

Remark 3 For homoclinic tangles, there is a well-defined dynamical pattern repeating itself periodically. However, for heteroclinic tangles, the repetitive dynamical pattern depends on two unstable eigenvalues. If they are rationally related, we have a repetitive pattern. If not, the repetitive pattern disappears.

3. Strange attractors in a class of duffing oscillator

In this section we study a nonlinear oscillator

$$\ddot{x} + (\alpha + \gamma x^2)\dot{x} + \beta x + \delta x^3 + \varepsilon[\eta x\dot{x} + (x^2-1)^2 \cos\omega t] = 0, \tag{7}$$

where $\alpha > 0$, γ, β, δ, and $\varepsilon > 0$, η, ω are parameters. We are interested in strange attractors for every $\varepsilon > 0$.

In history, many studies were carried out for Equation (7) on some parameters. For example, when $\varepsilon = 0$, Holmes and Rand (1980) studied its phase portrait and bifurcation set in (α,β) space. When $\gamma = \eta = 0, \varepsilon \neq 0$, Holmes (1979) discussed strange attractors with Poincaré map only for

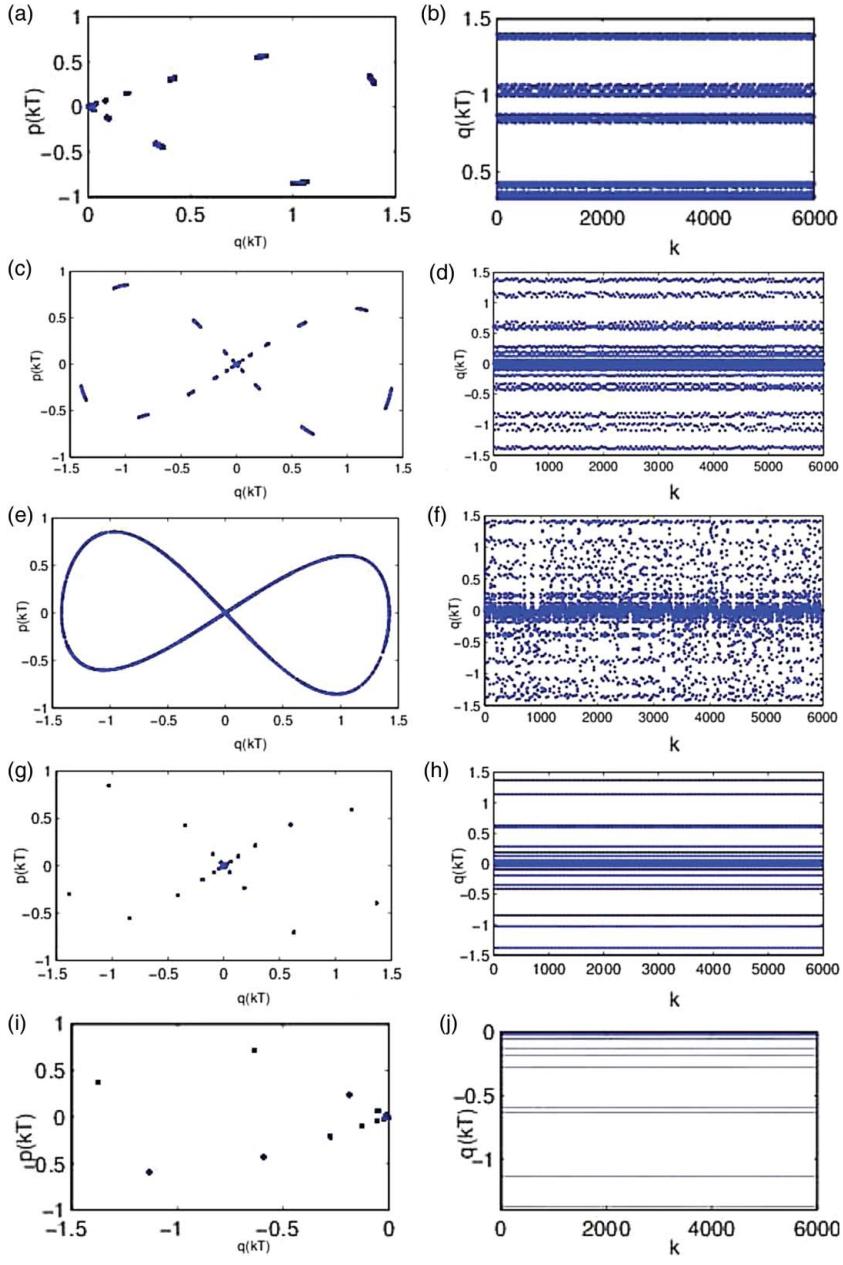

Figure 1. Case (i) of Equation (9). (a) One-sided Hénon-like attractor at $\varepsilon = 2.3 \times 10^{-4}$; (b) Time evolution of (a); (c) Two-sided Hénon-like attractor at $\varepsilon = 1.577 \times 10^{-4}$; (d) Time evolution of (c); (e) Two-sided rank one attractor at $\varepsilon = 3.2 \times 10^{-4}$; (f) Time evolution of (e); (g) Two-sided periodic sink at $\varepsilon = 3.3 \times 10^{-4}$; (h) Time evolution of (g); (m) One-sided periodic sink at $\varepsilon = 2.2 \times 10^{-4}$; and (n) Time evolution of (m).

certain ε. According to what we know, few studies are on strange attractors for every ε.

Write $\dot{x} = y$, Equation (7) becomes

$$\begin{aligned} \dot{x} &= y, \\ \dot{y} &= -\beta x - \delta x^3 - (\alpha + \gamma x^2)y \\ &\quad - \varepsilon[\eta xy + (x^2 - 1)^2 \cos \omega t]. \end{aligned} \tag{8}$$

We consider two cases for Equation (8). One case is $(\beta, \delta) = (-1, 1)$. In this case, we present dynamics of double homoclinic tangles. The other case is $(\beta, \delta) = (1, -1)$. This case leads to the heteroclinic tangles.

3.1. *Homoclinic tangles*

For $(\beta, \delta) = (-1, 1)$, Equation (8) simplifies to

$$\begin{aligned} \dot{x} &= y, \\ \dot{y} &= x - x^3 - (\alpha + \gamma x^2)y - \varepsilon[\eta xy + (x^2 - 1)^2 \cos \omega t]. \end{aligned} \tag{9}$$

Table 1. The dynamical pattern of Equation (9, case i).

$\alpha = 0.5, \gamma = -0.620831624826$
$\eta = 0.0, \omega = 2\pi$
Theoretical multiplicity $e^{\lambda_2} \approx 2.1832$

ε	Behavior type	Actual ratio
3.4×10^{-4}	HL(2)	–
3.3×10^{-4}	S(2)	–
3.2×10^{-4}	R(2)	–
2.3×10^{-4}	HL(1)	–
2.2×10^{-4}	S(1)	–
2.1×10^{-4}	R(2)	–
1.577×10^{-4}	HL(2)	2.1560
1.552×10^{-4}	S(2)	2.1263
1.477×10^{-4}	R(2)	2.1666
1.057×10^{-4}	HL(1)	2.1760
1.006×10^{-4}	S(1)	2.1869
1.000×10^{-4}	R(2)	2.1000
7.231×10^{-5}	HL(2)	2.1809
7.114×10^{-5}	S(2)	2.1816
6.775×10^{-5}	R(2)	2.1801
4.823×10^{-5}	HL(1)	2.1916
4.588×10^{-5}	S(1)	2.1927
4.586×10^{-5}	R(2)	2.1805
3.313×10^{-5}	HL(2)	2.1826
3.260×10^{-5}	S(2)	2.1822
3.104×10^{-5}	R(2)	2.1827
2.215×10^{-5}	HL(1)	2.1774
2.103×10^{-5}	S(1)	2.1816
2.101×10^{-5}	R(2)	2.1828
1.518×10^{-5}	HL(2)	2.1825
1.494×10^{-5}	S(2)	2.1821
1.422×10^{-5}	R(2)	2.1828
1.019×10^{-5}	HL(1)	2.1737
9.633×10^{-6}	S(1)	2.1831
9.629×10^{-6}	R(2)	2.1820
6.955×10^{-6}	HL(2)	2.1826
6.844×10^{-6}	S(2)	2.1829
6.517×10^{-6}	R(2)	2.1820
4.661×10^{-6}	HL(1)	2.1862
4.415×10^{-6}	S(1)	2.1818
4.411×10^{-6}	R(2)	2.1830

First, we need a dissipative saddle and homoclinic solution for the unperturbed equation

$$\begin{aligned} \dot{x} &= y, \\ \dot{y} &= x - x^3 - (\alpha + \gamma x^2)y. \end{aligned} \tag{10}$$

PROPOSITION 3.1 *For sufficiently small $\alpha > 0$, there is a γ_α such that Equation (10) has a saddle point $O(0,0)$ and two homoclinic solutions.*

Proof $O(0,0)$ is an equilibrium point of Equation (10) with eigenvalues

$$\lambda_1 = \frac{-\alpha - \sqrt{\alpha^2 + 4}}{2}, \quad \lambda_2 = \frac{-\alpha + \sqrt{\alpha^2 + 4}}{2}.$$

So, for $\alpha > 0$, we have $\lambda_1 < 0, \lambda_2 > 0$, and hence $O(0,0)$ is a saddle. Since $\lambda_1 + \lambda_2 = -\alpha < 0$, $O(0,0)$ is a dissipative saddle. The non-resonant is guaranteed by the irrational $\sqrt{\alpha^2 + 4}$.

For small $\alpha > 0$, we rewrite Equation (10) as

$$\begin{aligned} \dot{x} &= y, \\ \dot{y} &= x - x^3 - \alpha(1 + \gamma_\alpha x^2)y, \end{aligned} \tag{11}$$

where $\gamma_\alpha = \gamma/\alpha$. Equation (11) is an auto-perturbation of equation

$$\begin{aligned} \dot{x} &= y, \\ \dot{y} &= x - x^3. \end{aligned} \tag{12}$$

By simple computation, Equation (12) has two homoclinic solutions: $\ell_1(t) = \{(a_1(t), b_1(t)) : t \in \mathbb{R}\}$ and $\ell_2(t) = \{(-a_1(t), -b_1(t)) : t \in \mathbb{R}\}$, where

$$a_1(t) = \sqrt{2}\,\mathrm{sech}\, t, b_1(t) = -\sqrt{2}\mathrm{sech}\, t \cdot \tanh t.$$

The standard Melnikov function on $\ell_1(t)$ is

$$M_1 = \int_{-\infty}^{\infty} (1 + \gamma_\alpha a_1^2(t)) b_1^2(t)\, \mathrm{d}t = \frac{4}{3} + \frac{16}{15}\gamma_\alpha. \tag{13}$$

Thus, we have $M_1 = 0$ at $\gamma_\alpha = -\frac{5}{4}$, and a new homoclinic solution arises for Equation (10). Denote this homoclinic solution as $\tilde{\ell}_1(t) = \{(\tilde{a}_1(t), \tilde{b}_1(t)) : t \in \mathbb{R}\}$. Note that $\tilde{\ell}_2(t) = \{(-\tilde{a}_1(t), -\tilde{b}_1(t)) : t \in \mathbb{R}\}$ is also a homoclinic solution for Equation (10). They are all homoclinic to $O(0,0)$. This completes the proof of Proposition 3.1. ■

In the following, we fix α, γ_α as in Proposition 3.1, and consider Equation (9):

$$\begin{aligned} \dot{x} &= y, \\ \dot{y} &= x - x^3 - \alpha(1 + \gamma_\alpha x^2)y - \varepsilon[\eta x y + (x^2 - 1)^2 \cos \omega t]. \end{aligned} \tag{14}$$

Comparing Equation (14) with Equation (1), we have $P(x,y,t) = 0$, $Q(x,y,t) = -[\eta x y + (x^2 - 1)^2 \cos \omega t]$. Therefore, the Melnikov function (4) on $\tilde{\ell}_1(t)$ is

$$\mathcal{W}_1(\theta) = A_1 \eta + \sqrt{B_1^2 + C_1^2}\, \cos(\omega\theta + \varphi_1), \tag{15}$$

where, for $(x,y) \in \tilde{\ell}_1(t)$,

$$\begin{aligned} A_1 &= \int_{-\infty}^{\infty} \frac{x y^2 \mathrm{e}^{-\int_0^t \mathbb{E}_{\tilde{\ell}_1}(s)\,\mathrm{d}s}}{\sqrt{y^2 + [x - x^3 - \alpha(1 + \gamma_\alpha x^2)y]^2}}\, \mathrm{d}t, \\ B_1 &= \int_{-\infty}^{\infty} \frac{(x^2 - 1)^2 y \mathrm{e}^{-\int_0^t \mathbb{E}_{\tilde{\ell}_1}(s)\,\mathrm{d}s} \cos \omega t}{\sqrt{y^2 + [x - x^3 - \alpha(1 + \gamma_\alpha x^2)y]^2}}\, \mathrm{d}t, \\ C_1 &= \int_{-\infty}^{\infty} \frac{(x^2 - 1)^2 y \mathrm{e}^{-\int_0^t \mathbb{E}_{\tilde{\ell}_1}(s)\,\mathrm{d}s} \sin \omega t}{\sqrt{y^2 + [x - x^3 - \alpha(1 + \gamma_\alpha x^2)y]^2}}\, \mathrm{d}t, \\ \tan \varphi_1 &= \frac{C_1}{B_1}, \end{aligned} \tag{16}$$

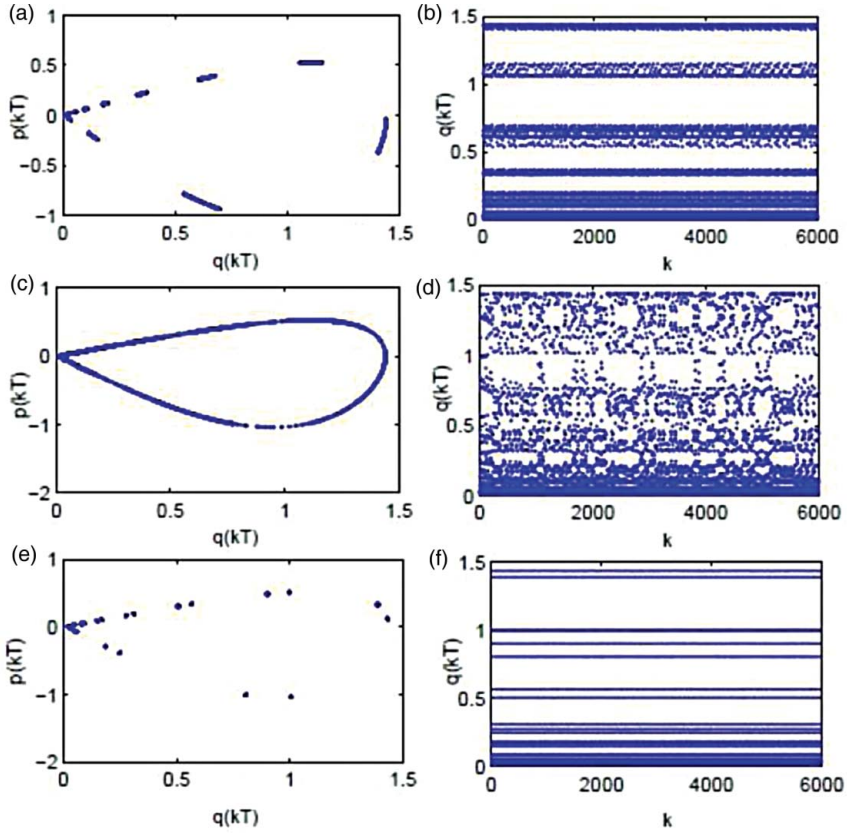

Figure 2. Case (v) of Equation (9). (a) One-sided Hénon-like attractor at $\varepsilon = 5.8 \times 10^{-3}$; (b) Time evolution of (a); (c) One-sided rank one attractor at $\varepsilon = 4.2 \times 10^{-3}$; (d) Time evolution of (c); (e) One-sided periodic sink at $\varepsilon = 5.1 \times 10^{-3}$; and (f) Time evolution of (e).

and

$$\mathbb{E}_{\tilde{\ell}_1}(t) = \tau^{\perp}_{\ell_1}(t) \begin{pmatrix} 0 & 1 \\ 1 - 3x^2 - 2\alpha\gamma_\alpha xy & -\alpha(1+\gamma_\alpha x^2) \end{pmatrix} \tilde{\tau}^{\perp}_{\ell_1}(t),$$

with

$$\tau^{\perp}_{\ell_1}(t) = \frac{(x - x^3 - \alpha(1+\gamma_\alpha x^2)y,\ -y)}{\sqrt{y^2 + [x - x^3 - \alpha(1+\gamma_\alpha x^2)y]^2}}.$$

Since $\tilde{\ell}_2(t) = -\tilde{\ell}_1(t)$, $t \in \mathbb{R}$, the Melnikov function on $\tilde{\ell}_2(t)$ is

$$\mathcal{W}_2(\theta) = -A_1\eta + \sqrt{B_1^2 + C_1^2}\cos(\omega\theta + \varphi_1). \tag{17}$$

From Equations (15) and (17), the four extrema of $\mathcal{W}_1(\theta), \mathcal{W}_2(\theta)$ are

$$M_1 = A_1\eta + \sqrt{B_1^2 + C_1^2},$$
$$m_1 = A_1\eta - \sqrt{B_1^2 + C_1^2},$$
$$M_2 = -A_1\eta + \sqrt{B_1^2 + C_1^2},$$
$$m_2 = -A_1\eta - \sqrt{B_1^2 + C_1^2}.$$

With Theorem 2.2, only two cases (i): $m_1 < 0 < M_1, m_2 < 0 < M_2$, and (v): $m_1 > 0, M_2 < 0$ or $m_2 > 0$, $M_1 < 0$ hold for real η. Solve case (i), we have

$$-\frac{\sqrt{B_1^2 + C_1^2}}{A_1} < \eta < \frac{\sqrt{B_1^2 + C_1^2}}{A_1}. \tag{18}$$

Solve case (v) of $m_1 > 0, M_2 < 0$, we have

$$\eta > \frac{\sqrt{B_1^2 + C_1^2}}{A_1}, \tag{19}$$

and from $m_2 > 0, M_1 < 0$, we have

$$\eta < -\frac{\sqrt{B_1^2 + C_1^2}}{A_1}. \tag{20}$$

With Theorem 2.2(i), for η in Equation (18), Equation (9) exhibits mixture of two homoclinic tangles. Consequently, both one-sided and two-sided Hénon-like attractors, rank one attractors, and periodic sinks occur for Equation (9), see Figure 1. The corresponding dynamical pattern is listed in Table 1, which repeats itself with period $e^{\lambda_2} \approx 2.1832$. The symbols "HL(1), HL(2)" stand for respectively one-sided and two-sided Hénon-like attractors. The same meaning also applies to symbols "S(1), S(2), R(1), R(2)." For η in Equation (19) or Equation (20), Theorem 2.2(v) tells us

Table 2. The dynamical pattern of Equation (9, case v).

$\alpha = 1.0, \gamma = -1.219038499970$
$\eta = 0.3, \omega = 2\pi$
Theoretical multiplicity $e^{\lambda_2} \approx 1.85527$

ε	Behavior type	Actual ratio
5.8×10^{-3}	HL(1)	–
5.1×10^{-3}	S(1)	–
4.4×10^{-3}	HL(1)	–
4.2×10^{-3}	R(1)	–
3.8×10^{-3}	S(1)	–
3.7×10^{-3}	R(1)	–
3.6×10^{-3}	HL(1)	–
3.4×10^{-3}	S(1)	–
3.3×10^{-3}	HL(1)	–
3.2×10^{-3}	S(1)	–
3.167×10^{-3}	HL(1)	1.8314
2.782×10^{-3}	S(1)	1.8332
2.389×10^{-3}	HL(1)	1.8418
2.283×10^{-3}	R(1)	1.8397
2.051×10^{-3}	S(1)	1.8528
1.999×10^{-3}	R(1)	1.8509
1.958×10^{-3}	HL(1)	1.8396
1.847×10^{-3}	S(1)	1.8408
1.819×10^{-3}	HL(1)	1.8142
1.746×10^{-3}	S(1)	1.8328
1.707×10^{-3}	HL(1)	1.8553
1.499×10^{-3}	S(1)	1.8559
1.288×10^{-3}	HL(1)	1.8548
1.230×10^{-3}	R(1)	1.8561
1.104×10^{-3}	S(1)	1.8578
1.099×10^{-3}	R(1)	1.8189
1.054×10^{-3}	HL(1)	1.8577
9.949×10^{-4}	S(1)	1.8565
9.832×10^{-4}	HL(1)	1.8501
9.403×10^{-4}	S(1)	1.8569
9.195×10^{-4}	HL(1)	1.8564
8.054×10^{-4}	S(1)	1.8612
6.929×10^{-4}	HL(1)	1.8589
6.629×10^{-4}	R(1)	1.8555
5.947×10^{-4}	S(1)	1.8564
5.916×10^{-4}	R(1)	1.8577
5.678×10^{-4}	HL(1)	1.8563
5.359×10^{-4}	S(1)	1.8565
5.296×10^{-4}	HL(1)	1.8565
5.063×10^{-4}	S(1)	1.8572

only one rank one attractor for Equation (9). Therefore, one-sided Hénon-like attractors, one-sided rank one attractors, and one-sided periodic sinks emerge expectedly, see Figure 2. Table 2 is the corresponding dynamical pattern.

3.2. *Heteroclinic tangles*

For $(\beta, \delta) = (1, -1)$, Equation (8) is changed to

$$\begin{aligned} \dot{x} &= y, \\ \dot{y} &= -x + x^3 - (\alpha + \gamma x^2)y - \varepsilon[\eta xy + (x^2 - 1)^2 \cos \omega t]. \end{aligned} \tag{21}$$

To apply Theorem 2.3 to Equation (21), we need two heteroclinic solutions together with two saddles for unperturbed equation

$$\begin{aligned} \dot{x} &= y, \\ \dot{y} &= -x + x^3 - (\alpha + \gamma x^2)y. \end{aligned} \tag{22}$$

PROPOSITION 3.2 *For sufficiently small $\alpha > 0$, there is a γ_α such that Equation (22) has two heteroclinic solutions associated with two saddles $O_1(-1, 0)$ and $O_2(1, 0)$, which are dissipative and non-resonant.*

Proof $O_1(-1, 0)$ and $O_2(1, 0)$ are two equilibrium points of Equation (22), sharing the same eigenvalues

$$\lambda_1 = \frac{-\alpha - \gamma - \sqrt{(\alpha + \gamma)^2 + 8}}{2},$$
$$\lambda_2 = \frac{-\alpha - \gamma + \sqrt{(\alpha + \gamma)^2 + 8}}{2}.$$

For $\alpha + \gamma > 0$, we have $\lambda_1 < 0, \lambda_2 > 0$. So $O_1(-1, 0)$ and $O_2(1, 0)$ are both saddles. Since $\lambda_1 + \lambda_2 = -(\alpha + \gamma) < 0$, they are simultaneously dissipative. Moreover, they are both non-resonant due to the irrational $\sqrt{(\alpha + \gamma)^2 + 8}$.

For small $\alpha > 0$, Equation (22) is also equivalent to

$$\begin{aligned} \dot{x} &= y, \\ \dot{y} &= -x + x^3 - \alpha(1 + \gamma_\alpha x^2)y, \end{aligned} \tag{23}$$

which perturbs from equation

$$\begin{aligned} \dot{x} &= y, \\ \dot{y} &= -x + x^3. \end{aligned} \tag{24}$$

Clearly, Equation (24) has two heteroclinic solutions with symmetry: $\ell(t) = \{(a(t), b(t)) : t \in \mathbb{R}\}$ and $\ell_*(t) = \{(-a(t), -b(t)) : t \in \mathbb{R}\}$, where

$$a(t) = \tanh\left(\frac{\sqrt{2}}{2}t\right), \quad b(t) = \frac{\sqrt{2}}{2}\operatorname{sech}^2\left(\frac{\sqrt{2}}{2}t\right).$$

The standard Melnikov function on $\ell(t)$ is

$$M = \int_{-\infty}^{\infty} (1 + \gamma_\alpha a^2(t))b^2(t)\, dt = \frac{2\sqrt{2}}{3} + \frac{2\sqrt{2}}{15}\gamma_\alpha. \tag{25}$$

So $M = 0$ at $\gamma_\alpha = -5$, and thus a new heteroclinic solution arises for Equation (23). Denote this heteroclinic solution as $\tilde{\ell}(t) = \{(\tilde{a}(t), \tilde{b}(t)) : t \in \mathbb{R}\}$. Easy to check that

$\tilde{\ell}_*(t) = \{(-\tilde{a}(t), -\tilde{b}(t)) : t \in \mathbb{R}\}$ is also a heteroclinic solution for Equation (23). They are both heteroclinic to saddles $O_1(-1,0)$ and $O_2(1,0)$. This confirms Proposition 3.2. ■

For Equation (21), two Melnikov functions on $\tilde{\ell}(t), \tilde{\ell}_*(t)$ are

$$\begin{aligned} \mathcal{W}(\theta) &= A\eta + \sqrt{B^2 + C^2}\cos(\omega\theta + \varphi), \\ \mathcal{W}_*(\theta) &= -A\eta + \sqrt{B^2 + C^2}\cos(\omega\theta + \varphi), \end{aligned} \tag{26}$$

where, for $(x,y) \in \tilde{\ell}(t)$,

$$\begin{aligned} A &= \int_{-\infty}^{\infty} \frac{xy^2 \mathrm{e}^{-\int_0^t \mathbb{E}_{\tilde{\ell}}(s)\,\mathrm{d}s}}{\sqrt{y^2 + [-x + x^3 - \alpha(1+\gamma_\alpha x^2)y]^2}}\,\mathrm{d}t, \\ B &= \int_{-\infty}^{\infty} \frac{(x^2-1)^2 y \mathrm{e}^{-\int_0^t \mathbb{E}_{\tilde{\ell}}(s)\,\mathrm{d}s}\cos\omega t}{\sqrt{y^2 + [-x + x^3 - \alpha(1+\gamma_\alpha x^2)y]^2}}\,\mathrm{d}t, \\ C &= \int_{-\infty}^{\infty} \frac{(x^2-1)^2 y \mathrm{e}^{-\int_0^t \mathbb{E}_{\tilde{\ell}}(s)\,\mathrm{d}s}\sin\omega t}{\sqrt{y^2 + [-x + x^3 - \alpha(1+\gamma_\alpha x^2)y]^2}}\,\mathrm{d}t, \\ \tan\varphi &= \frac{C}{B}, \end{aligned} \tag{27}$$

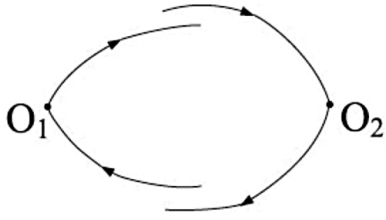

Figure 3. Case (v) of Equation (21).

Table 3. The dynamical pattern of Equation (21, case i).

$\alpha = -0.5, \gamma = 2.429857626335$
$\eta = 0, \omega = 2\pi$
Theoretical multiplicity $\mathrm{e}^{\lambda_2} \approx 2.0793$

ε	Behavior type	Actual ratio
3.7×10^{-3}	Hénon-like attractors	–
3.6×10^{-3}	Periodic sinks	–
3.5×10^{-3}	Transient tangles	–
1.772×10^{-3}	Hénon-like attractors	2.0880
1.749×10^{-3}	Periodic sinks	2.0583
1.669×10^{-3}	Transient tangles	2.0971
8.386×10^{-4}	Hénon-like attractors	2.1130
8.276×10^{-4}	Periodic sinks	2.1133
7.896×10^{-4}	Transient tangles	2.1137
3.960×10^{-4}	Hénon-like attractors	2.1177
3.900×10^{-4}	Periodic sinks	2.1221
3.728×10^{-4}	Transient tangles	2.1180
1.864×10^{-4}	Hénon-like attractors	2.1245
1.839×10^{-4}	Periodic sinks	2.1207
1.753×10^{-4}	Transient tangles	2.1266
8.710×10^{-5}	Hénon-like attractors	2.1401
8.595×10^{-5}	Periodic sinks	2.1396
8.175×10^{-5}	Transient tangles	2.1443

and

$$\mathbb{E}_{\tilde{\ell}}(t) = \tau_{\tilde{\ell}}^{\perp}(t) \begin{pmatrix} 0 & 1 \\ 3x^2 - 1 - 2\alpha\gamma_\alpha xy & -\alpha(1+\gamma_\alpha x^2) \end{pmatrix} \tilde{\tau}_{\tilde{\ell}}^{\perp}(t),$$

with

$$\tau_{\tilde{\ell}}^{\perp}(t) = \frac{(-x + x^3 - \alpha(1+\gamma_\alpha x^2)y,\ -y)}{\sqrt{y^2 + [-x + x^3 - \alpha(1+\gamma_\alpha x^2)y]^2}}.$$

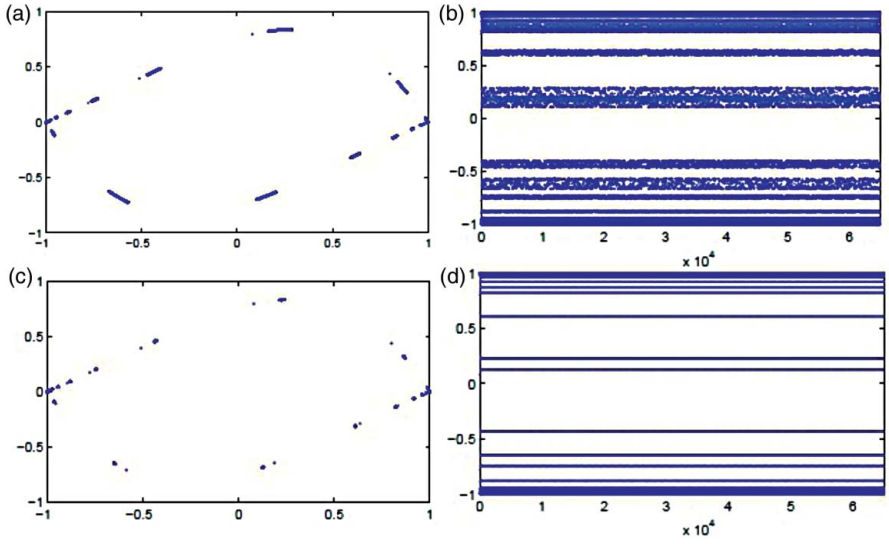

Figure 4. Case (i) of Equation (21). (a) Hénon-like attractor at $\varepsilon = 8.710 \times 10^{-5}$; (b) Time evolution of (a); (c) Periodic sink at $\varepsilon = 3.900 \times 10^{-5}$; and (d) Time evolution of (c).

The four extrema of $\mathcal{W}(\theta), \mathcal{W}_*(\theta)$ are $M = A\eta + \sqrt{B^2 + C^2}$, $m = A\eta - \sqrt{B^2 + C^2}$, $M_* = -A\eta + \sqrt{B^2 + C^2}$, $m_* = -A\eta - \sqrt{B^2 + C^2}$. With the same reason, only two cases hold for real η: (i) $m < 0 < M, m_* < 0 < M_*$; (v) $m > 0, M_* < 0$ or $m_* > 0, M < 0$. However, for heteroclinic tangles, there is no return map corresponding to case (v), see Figure 3. Therefore, only case (i) make sense. Without loss of generality, we assume $A > 0$. Then case (i) implies

$$-\frac{\sqrt{B^2 + C^2}}{A} < \eta < \frac{\sqrt{B^2 + C^2}}{A}. \tag{28}$$

Take η satisfying Equation (28), from Theorem 2.3 we have H*é*non-like attractors and periodic sinks, see Figure 4. Horseshoes are there, but we can not visualize it in numerical simulations. Table 3 is a dynamical pattern for Equation (21) when $\alpha = -0.5, \gamma = 2.42985626335$, $\eta = 0$.

4. Conclusions

In this paper, H*é*non-like attractors, rank one attractors, and periodic sinks are obtained in a class of Duffing oscillator. Among the three attractors, Hénon-like attractors and rank one attractors are chaotic in the sense of the SRB measure. All the three attractors are organized in an invariant pattern that repeats itself periodically with respect to the forcing magnitude ε as $\varepsilon \to 0$.

Acknowledgements

The authors thank Prof. Jibin Li and Prof. Fangyue Chen for their encouragement and generous support. This paper is supported by a NSFC grant (No. 11171309).

References

Benedicks, M., & Young, L. S. (1993). Sinai-Bowen-Ruelle measure for certain Hénon maps. *Inventiones Mathematicae*, *112*, 514–576.

Chen, F. J., Oksasoglu, A., & Wang, Q. D. (2013). Heteroclinic tangles in time-periodic equations. *Journal of Differential Equations*, *254*, 1137–1171.

Holmes, P. (1979). A nonlinear oscillator with a strange attractor. *The Philosophical Transactions of the Royal Society of London*, Series A, *292*, 419–448.

Holmes, P., & Rand, D. (1980). Phase portraits and bifurcations of the non-linear oscillator: $\ddot{x} + (\alpha + \gamma x^2)\dot{x} + \beta x + \delta x^3 = 0$. *Journal Non-linear Mechanics*, *15*, 449–458.

Poincaré, H. (1899). Les *Méthodes* Nouvelles de la *Mécanique Céleste*. 3 vols. Paris: Gauthier-Villars.

Wang, Q. D. (2009). *Periodically forced double homoclinic loops to a dissipative saddle*. Unpublished manuscript.

Wang, Q. D. (2011). *Dynamics of non-autonomously perturbed homoclinic solutions*. Unpublished manuscript.

Wang, Q. D., & Oksasoglu, A. (2008). Rank one chaos: theory and applications. *International Journal of Bifurcation Chaos*, *18*, 1261–1319.

Wang, Q. D., & Oksasoglu, A. (2010). Periodic occurrence of chaotic behavior of homoclinic tangles. *Physica D: Nonlinear Phenomena*, *239*, 387–395.

Wang, Q. D., & Oksasoglu, A. (2011). Dynamics of homoclinic tangles in periodically perturbed second-order equations. *Journal of Differential Equations*, *250*, 710–751.

Young, L. S. (2002). What are SRB measure, and which dynamical systems have them? *Journal of Statistical Physics*, *108*, 733–754.